Synthesis of carbon nanotubes-Fe-Al2O3 powders.Influence of the characteristics of the starting Al1.8Fe0.2O3 oxide solid solution

Christophe Laurent, Alain Peigney, Emmanuel Flahaut, Abel Rousset

Synthesis of carbon nanotubes–Fe–Al_2O_3 powders. Influence of the characteristics of the starting $Al_{1.8}Fe_{0.2}O_3$ oxide solid solution

Ch. Laurent*, A. Peigney, E. Flahaut, A. Rousset

Laboratoire de Chimie des Matériaux Inorganiques, ESA CNRS 5070, Université Paul-Sabatier, 31062 Toulouse Cedex 4, France

Abstract

$Al_{1.8}Fe_{0.2}O_3$ amorphous solid solution have been calcined at temperatures between 1025 and 1100°C and the obtained powders have been reduced in a H_2–CH_4 gas mixture (12 mol% CH_4) at 1050°C in order to prepare carbon nanotubes (C_{NTs})–Fe/Fe_3C–Al_2O_3 nanocomposite powders. The calcination at 1100°C leads to powders containing an α-$Al_{2-2x}Fe_{2x}O_3$ solid solution ($x < 0.1$) and some traces of a Fe-rich phase (α-$Fe_{2-2y}Al_{2y}O_3$) that gives, under reduction, large Fe particles which catalyze the growth of ribbon like filaments. An α-$Al_{1.8}Fe_{0.2}O_3$ monophased solid solution with a higher specific surface area is obtained after a calcination at only 1050 or 1025°C. In the corresponding composite powders, all filaments are isolated C_{NTs} or bundles of C_{NTs} and the high specific area is beneficial to both the quantity and the quality parameters which are greatly enhanced in comparison with previous results. About 20% of the observed C_{NTs} are single wall nanotubes (SWNTs). The majority of the observed multiwall nanotubes (MWNTs) have only two walls and the inner diameters are distributed between 0.8 and 6 nm, with a peak at 2 nm. The in-situ catalysis by selective reduction of a solid solution allows for production of nanocomposite powders containing very large quantities of high quality C_{NTs}.

Keywords: A. Composites; A. Fullerenes; A. Nanostructures; A. Oxides; B. Chemical synthesis

* Corresponding author. Tel.: +33-5-61-55-61-22; fax: +33-5-61-55-61-63.
E-mail address: laurent@ups-tlse.fr (Ch. Laurent).

1. Introduction

Carbon nanotubes [1] (hereafter denoted as C_{NTs}) have truly unique properties due to both their particular structure and nanometric diameter. A comprehensive description of the structure and properties and an early grasp of the potential applications of C_{NTs} are given in the book by Dresselhaus et al. [2]. The various synthesis routes involving the use of metal catalysts have been reviewed by Laurent et al. [3]. In particular, chemical methods such as the catalytic decomposition of hydrocarbons on metal particles (Fe, Co, Ni) produce Iijima-type C_{NTs} when the catalytic particles are sufficiently small [4–8]. The main difficulty is to obtain catalyst particles with a size that is nanometric at the relatively high temperature (usually higher than 800°C) required for the formation of C_{NTs}. To achieve this, the present authors have proposed an original catalytic method based on the selective reduction of $Al_{2-2x}Fe_{2x}O_3$ solid solutions [9]. Metal nanoparticles are formed upon reduction in H_2–CH_4 both inside the matrix grains and at their surface [10] but only the latter are able to react with CH_4. Moreover, these pristine Fe (and/or Fe_3C) nanoparticles have a size adequate for the in-situ catalytic formation of C_{NTs}. An analysis method has been proposed [9] in order to characterize the obtained C_{NTs}–Fe/Fe_3C–Al_2O_3 composite powders at a macroscopical scale and thus produce data more representative of the material than those derived from local techniques. Previous investigations have shown that it is necessary to use $Al_{2-2x}Fe_{2x}O_3$ solid solutions which firstly are crystallized in the stable α (corundum) form [11] and secondly are monophased [12]. Powders containing 10 cat.% Fe and calcined during 2 h at 1100°C generally meet these two requirements. However, we detected that some batches of such powders lead, after reduction, to composite powders which present a quality lower than that usually obtained by reduction of a monophased oxide solid solution. On the other hand, in order to maximize the quantity of C_{NTs}, it is obviously desirable that there are more surface nanoparticles. For a given Fe content, this could be achieved by using a starting solid solution with a higher specific surface area, since this will result in a higher proportion of Fe^{3+} ions located at the surface rather than in the bulk of the oxide grains. One of the essential elaboration parameters that settle both the structure and the specific surface area of these powders is the calcination temperature. Thus, we study in this work the influence of the calcination temperature, in order to reach an α-$Al_{1.8}Fe_{0.2}O_3$ monophased solid solution with the highest specific surface area possible. The consequences on the characteristics of the C_{NTs}–Fe/Fe_3C–Al_2O_3 composite powders obtained after reduction are also investigated.

2. Experimental

An amorphous $Al_{1.8}Fe_{0.2}O_3$ solid solution was prepared by decomposition in air (400°C, 2 h) of the corresponding mixed oxalate. The powder was divided into four parts, which were submitted to different calcination treatments in air, in order to obtain powders of different specific surface areas composed of an α-$Al_{1.8}Fe_{0.2}O_3$ solid solution. The oxides, denoted as OA1, OA2, OA3, and OA4 hereafter, were prepared by calcination at 1025°C for 10 min, at 1050°C for 10 min, at 1100°C for 10 min and at 1100°C for 60 min, respectively. A part of powder OA4 was attritor-milled to decrease its grain size and thus increase its specific

surface area (specimen OB). Parts of the powders were reduced in H_2–CH_4 gas mixture (12 mol% CH_4) at 1050°C for 60 min, producing to the C_{NTs}–Fe/Fe_3C–Al_2O_3 powders. The gas flow was dried on P_2O_5 and its composition was set up using massflow controllers. The flow rate was fixed at 250 sccm. The composite powders are denoted CA1, ..., CA4, and CB in the following sections.

The powders were studied using scanning and transmission electron microscopy (SEM and TEM) and by X-ray diffraction (XRD) using Cu Kα radiation ($\lambda = 0.15418$ nm). Parts of the reduced powders were oxidized in air at 900°C in order to eliminate all the carbon, as required for the specific surface area study. The specific surface areas of the oxide powders (S_{ss}), of the reduced powders (S_n) and of the specimens oxidized at 900°C (S_{on}) were measured by the BET method using N_2 adsorption at liquid N_2 temperature. We used a Micromeritics FlowSorb II 2300 apparatus that gives a specific surface area value from one point (i.e., one adsorbat pression) and requires calibration. We determined that the reproducibility of the results is in the ±3% range. The carbon content in the reduced powders was determined by flash combustion with an accuracy of ±2%. In addition, some oxide powders (OA2 and OA4) were studied by ^{57}Fe Mössbauer spectroscopy. The Mössbauer spectra were recorded at room temperature with a constant acceleration spectrometer using a 50 mCi ^{57}Co (Rh) source; the spectrometer was calibrated by collecting at room temperature the spectrum of a standard Fe foil and the center shift (CS) values quoted hereafter are with reference to this standard.

3. Results

3.1. Oxide powders

The XRD patterns of the oxide powders show the peaks of the desired α-$Al_{2-2x}Fe_{2x}O_3$ ($x \approx 0.1$) solid solution. The peaks are narrow, reflecting a high crystallization level, with no difference observable from one powder to the other. However, α-Fe_2O_3 is detected on the patterns of the three specimens calcined at 1100°C, in an extremely small proportion for OA3 and a little higher one for OA4 and OB.

Analysis of the Mössbauer spectra recorded for OA2 and OA4 (Fig. 1) supports the XRD results. Indeed, only a doublet (CS = 0.30 mm/s, quadrupole splitting (ΔE_Q) = 0.54 mm/s, half-line-width (HLW) = 0.18 mm/s) corresponding to paramagnetic Fe^{3+} ions substituting for Al^{3+} ions in the corundum lattice is observed for OA2. In contrast, a sextet (CS = 0.36 mm/s, hyperfine field = 505 kG, HLW = 0.22 mm/s) accounting for a α-Fe_2O_3 phase (probably partly substituted by Al^{3+} ions) is detected in addition to the doublet (CS = 0.30 mm/s, ΔE_Q = 0.53 mm/s, HLW = 0.18 mm/s) for OA4. The proportion of the sextet represents ca. 8% of the total Fe species. It thus appears that increasing the calcination temperature or time provokes some phase partitioning between an α-Al_2O_3-rich solid solution (major phase) and an α-Fe_2O_3-rich solid solution (minor phase). The composition of the desired solid solution (α-$Al_{1.8}Fe_{0.2}O_3$) is indeed close to the solubility limit of α-Fe_2O_3 in α-Al_2O_3 [13–15], which also depends on the temperature.

The specific surface area (S_{ss}, Table 1) of the OA oxide powders decreases upon the

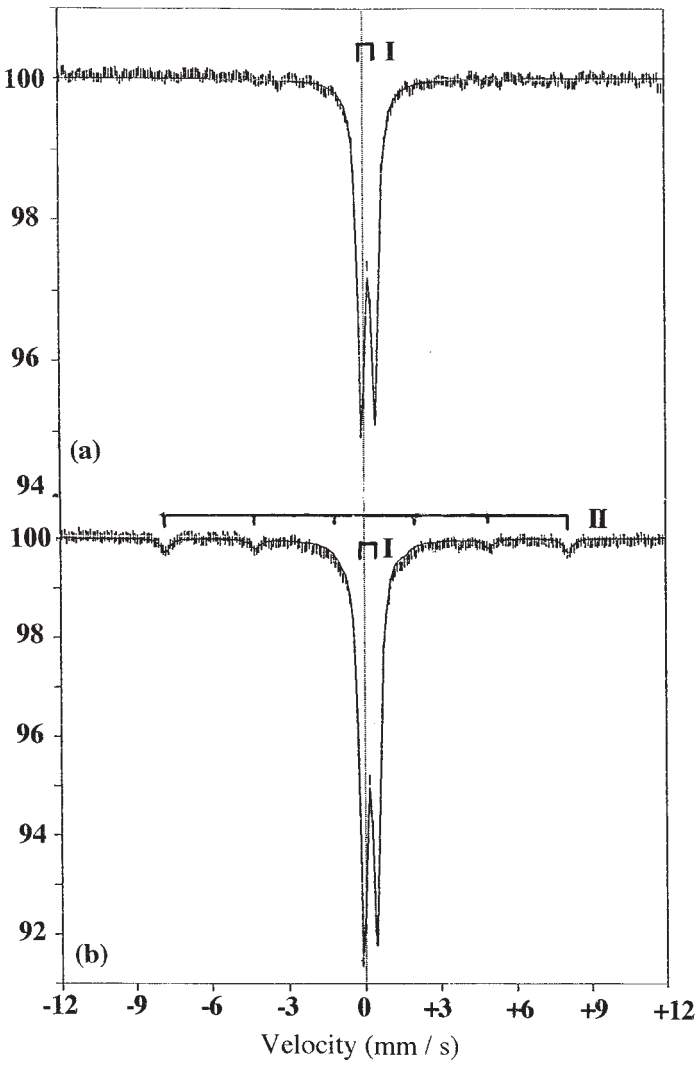

Fig. 1. Mössbauer spectra of the OA2 (a) and OA4 (b) oxide powders. I: paramagnetic Fe^{3+}; II: α-Fe_2O_3.

Table 1
Specific surface area of the starting solid solutions (S_{ss}) and some characteristics of the powders containing carbon nanotubes: carbon content (C_n) and specific surface areas [S_n, value measured for the nanocomposite powders; S_{on}, value measured for the powders oxidized at 900°C; $\Delta S = S_n - S_{on}$, the quantity of carbon nanotubes (see text); $\Delta S/C_n$, representing the carbon quality (see text)]

Specimen	Calcination T (°C), t (min)	S_{ss} m^2/g	Specimen	C_n (wt%)	S_n m^2/g	S_{on} m^2/g	ΔS m^2/g	$\Delta S/C_n$ m^2/g
OA1	1025, 60	8.1	CA1	6.23	27.0	7.5	19.6	314
OA2	1050, 10	6.7	CA2	5.99	20.7	6.7	13.9	232
OA3	1100, 10	5.3	CA3	6.02	18.5	5.4	13.1	218
OA4	1100, 60	3.6	CA4	5.84	15.2	4.4	10.7	183
OB	1100, 60	11.8	CB	5.79	19.4	9.4	10.1	174

increase of the calcination temperature or time. Attrition-milling (specimen OB) provokes a threefold increase of the specific surface area compared to the parent powder (OA4). SEM observations show that the OA powders are composed of grains up to 10 μm large and that the grains are submicronic in OB. It is thus important to note that differences between the OA powders mostly reflect changes in the surface porosity, whereas differences between OA4 and OB reflect a change in the geometrical surface.

3.2. Composite powders

The XRD patterns of the reduced powders are similar to each other. Besides the corundum peaks, accounting for α-Al_2O_3 or a partially reduced α-$Al_{2-2x}Fe_{2x}O_3$ ($x \leq 0.1$) solid solution, α-Fe and Fe_3C are detected in all the powders, with similar proportions from one powder to the other. γ-Fe may be present in all or some powders, but is extremely difficult to detect on the XRD patterns because the γ-Fe (111) diffraction peak ($d_{111} = 0.208$ nm) is probably masked by the basis of the corundum (113) peak (d_{113}) = 0.209 nm), the more so if Fe_3C ($d_{121} = 0.210$ nm) is present as well. Previous Mössbauer spectroscopy studies of similar composite powders have revealed the presence of a nonferromagnetic Fe phase (γ-Fe or Fe–C alloy) in addition to α-Fe and Fe_3C [11,16].

The carbon contents (C_n, Table 1) are in the 5.8–6.2 wt% range. For the CA powders, a slight increase is observed when the specific surface area of the starting powder increases (from OA4 to OA1). However, in the CB powder, the carbon content is not higher than in CA4, showing that the increase of S_{ss} due to the attrition milling of the starting oxide solution does not contribute to increase the amount of carbon deposited during the reduction.

The specific surface area of the nanocomposite powders (S_n, Table 1) is higher than the specific surface area of the starting solid solutions (S_{ss}, Table 1). As pointed out earlier [9,11] it is the deposition of carbon in the composite powder, particularly in the form of C_{NTs}, which is responsible for most of this supplementary surface area. The Fe and/or Fe_3C particles which form at the surface of the matrix grains can also contribute to this increase of surface area, but to a much smaller extent. After all the carbon is eliminated by air oxidation at 900°C, the specific surface area of the resulting powders (S_{on}, Table 1) is similar or slightly lower than those of the starting solid solutions (S_{ss}, Table 1). For OA1 and OA2 which have been calcined for only 10 min at 1025 and 1050°C, respectively, some sintering of the matrix grains probably occurs during the reducing thermal treatment at 1050°C. Similarly, for OB, some sintering occurs because of the submicronic size of the grains.

As proposed in previous works [9,11], $\Delta S = S_n - S_{on}$ (Table 1) represents the surface area of the carbon in the nanocomposite powder, which essentially corresponds to that of the C_{NTs}, thus reflecting the quantity of C_{NTs} (more precisely of nanotube bundles). For CA powders, ΔS dramatically increases upon the decrease of the calcination temperature and time (from OA4 to OA1) and thus when the specific surface area of the starting oxide solid solution (S_{ss}) increases, from 10.7 ± 0.6 m^2/g for CA4 to 19.6 ± 1.0 m^2/g for CA1 (Fig. 2). By contrast, for CB, the ΔS value (10.1 ± 0.8 m^2/g) is similar to that measured for CA4. $\Delta S/C_n$ (Table 1 and Fig. 3) can be considered as a quality data, a higher figure for $\Delta S/C_n$ denoting a smaller average tube diameter and/or more carbon in tubular form and/or tubes with fewer walls [9,11]. For the CA specimens, as a consequence of the strong increase in

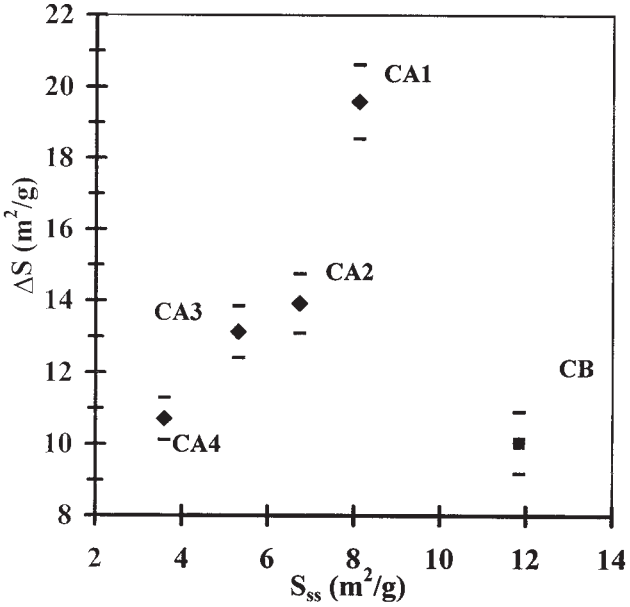

Fig. 2. $\Delta S = S_n - S_{on}$ vs. the specific surface area (S_{ss}) of the starting oxide.

ΔS and the almost unmodified C_n values when S_{ss} increases (Fig. 2, Table 1) $\Delta S/C_n$ also dramatically increases with S_{ss} (Fig. 3). For the CB specimen, in line with the results on ΔS and C_n, $\Delta S/C_n$ is similar to the one of CA4, in spite of the fact that OB has a specific surface area more than three times larger than OA4 (Table 1). Thus, it is obvious that, whereas the decreasing of the calcination temperature (and/or time) and the attrition milling both lead to a higher specific surface area of the starting oxide solid solution, the consequences on the characteristics of the carbon species deposited during reduction are very different.

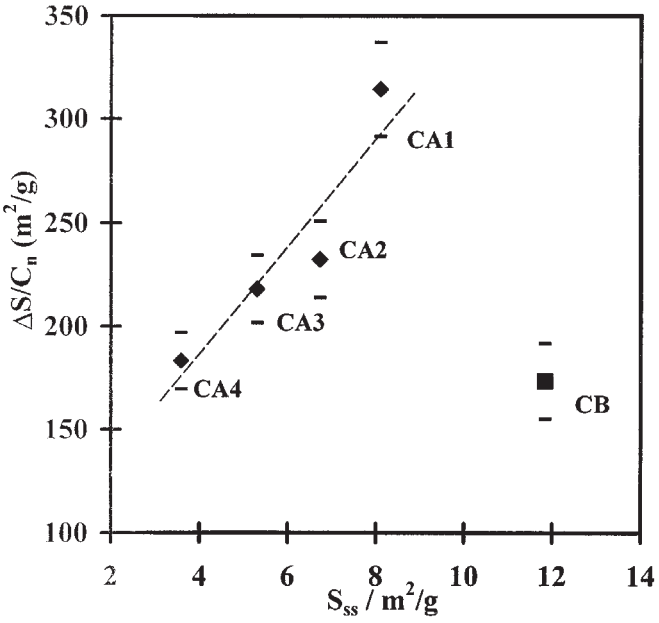

Fig. 3. $\Delta S/C_n$ vs. the specific surface area (S_{ss}) of the starting oxide. The dashed lines are guides to the eye.

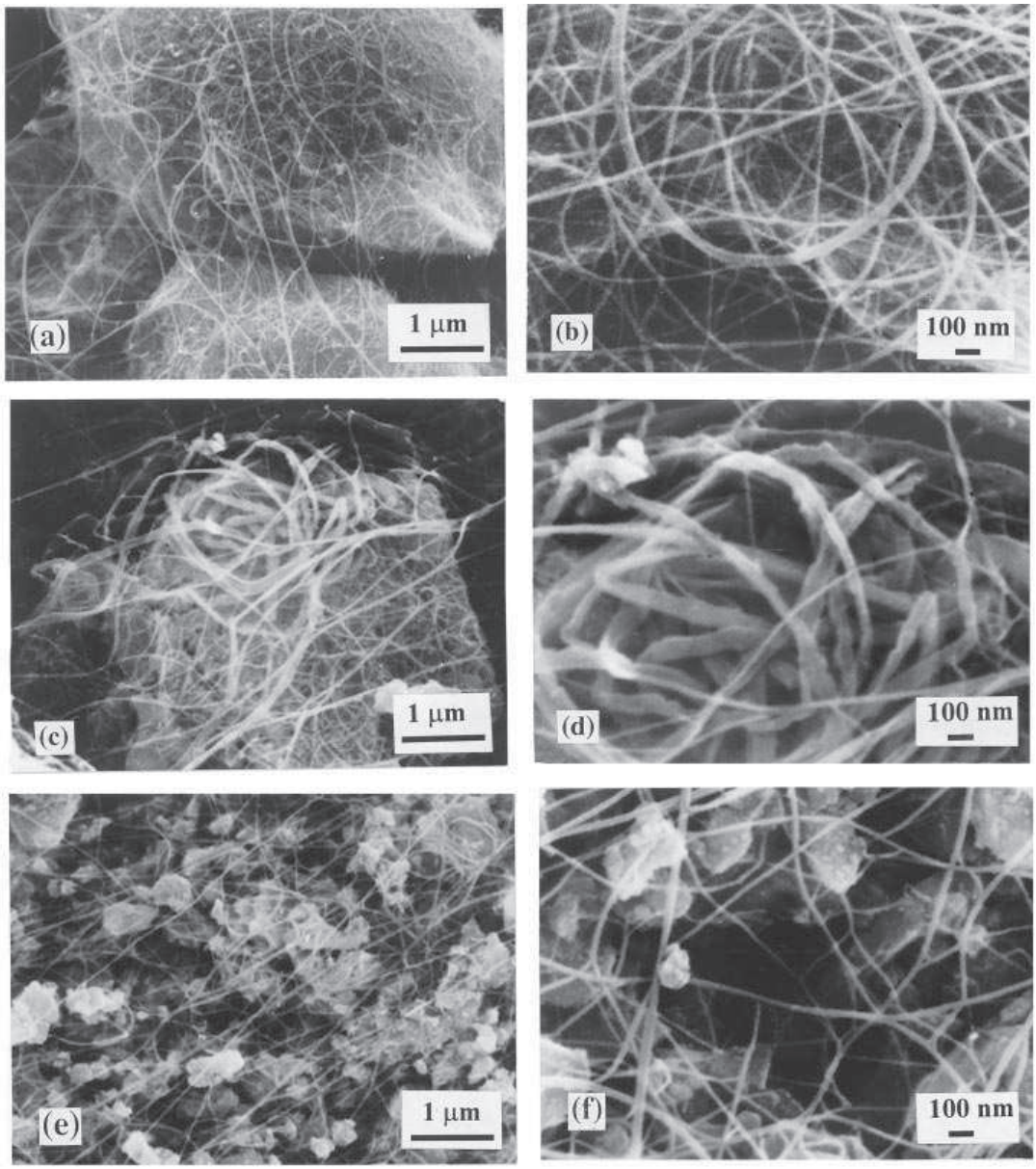

Fig. 4. SEM images of the nanocomposite powders: CA1 (a, b), CA4 (c, d), and CB (e, f).

3.3. Scanning electron microscopy

The CA1, CA4, and CB powders, prepared from the powders which presented the greatest S_{ss} differences, have been observed by SEM (Fig. 4a–f). These images show the web of filaments covering the matrix grains, which explains that the powders retain the shape of the reduction vessel when transferred to a storage box. In CA1 (Fig. 4a and b), long and flexible filaments, no more than 50 nm in diameter, are extensively branched one to each other and have a smooth and regular surface. HREM observations performed in previous works have shown that these filaments are in fact bundles of C_{NTs} [9,11,12,16]. In CA4 (Fig. 4c and d), in addition to these C_{NTs} bundles, some groups of much larger filaments, up to 200 nm wide, also locally appear on some matrix grains. The higher magnification image (Fig. 4d) shows

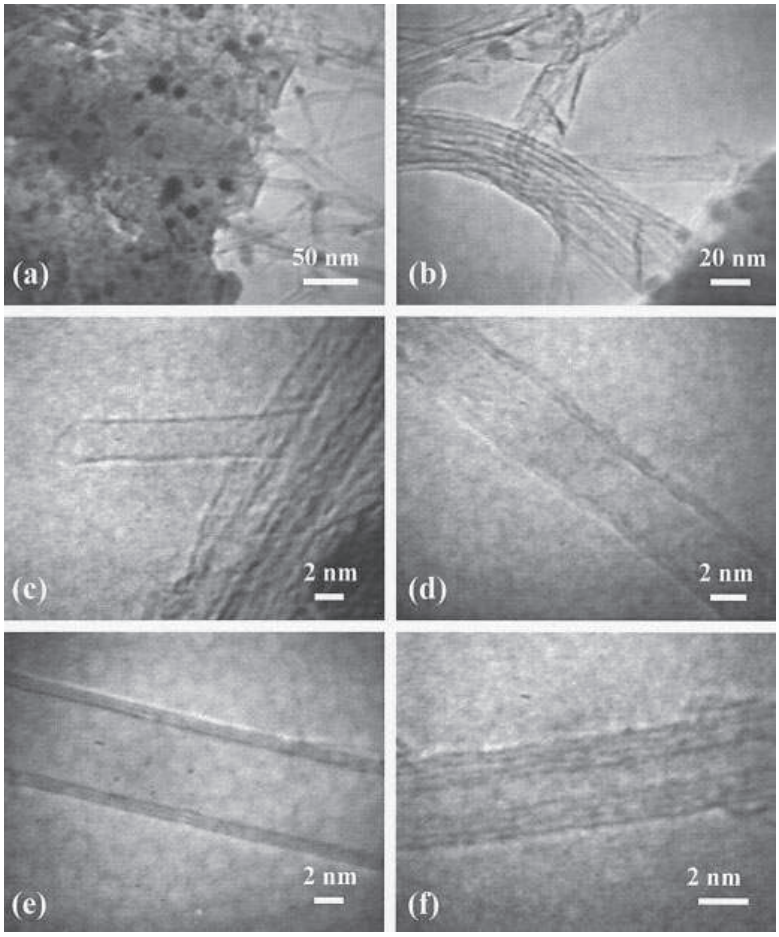

Fig. 5. TEM (a, b) and HREM (c, f) digital images of the CA1 (a, b, d–f) and CA4 (c) powders.

that these larger filaments look like ribbons, have irregular surfaces, and are less flexible than the bundles of C_{NTs} (Fig. 4b). No other difference has been found between CA1 and CA4. Other species such as thick, short tubes or spheroidal deposits [9,11,12,16] are only rarely observed. The CB powder (Fig. 4e and f) is composed of submicronic matrix grains entrapped in a web-like network of C_{NTs} bundles similar to those found in the CA4 specimen.

3.4. Transmission electron microscopy

TEM and HREM observations performed on the CA1 and CA4 powders reveal a similar feature. In Fig. 5a, some C_{NTs} are superimposed with a matrix grain and some Fe and/or Fe_3C nanoparticles (appearing as black dots), between 5 and 15 nm in diameter, which are located either at the matrix grain surface or in an intragranular position [10]. Fig. 5b shows several C_{NTs} bundles, the larger ones being 30 nm in diameter. It seems that they are made up of C_{NTs} thinner than 5 nm. Because the C_{NTs} are rarely aligned in the focus plane and also because the electron beam induces vibrations and sometimes a fast deterioration of the tubes, images with well-resolved and not deteriorated walls are difficult to obtain by HREM. A single wall nanotube (SWNT) about 2.5 nm in diameter, emerging out of a bundle, is observed in Fig. 5c. The next images show multiwall nanotubes (MWNTs) with two walls,

4 nm in outer diameter (Fig. 5d), where the waves on the walls are caused by the deterioration; with three walls, 7.1 nm in outer diameter (Fig. 5e); and with four walls, 3.4 nm in outer diameter (Fig. 5f). Very seldom were thick and short filaments, which sometimes have a bamboo shape [16], detected. Also, in both CA1 and CA4, some Fe and/or Fe_3C nanoparticles, in the 10–15 nm range, covered with a few graphene sheets were present at the surface of the matrix grains. Whatever the powders we observed in our previous studies [9,11,12,16], we always detected some of such particles. However, the precise nature of the nanoparticles (Fe, Fe_3C, or Fe–C alloy) that are catalytically active or not for the C_{NTs} formation has not been elucidated. The large filaments looking like ribbons that were detected by SEM in the CA4 powder were not observed by TEM, possibly because they were not retained during the TEM specimen preparation.

The distribution of the numbers of walls (Fig. 6a) and of the inner and outer diameters (Fig. 6b) was calculated from data obtained from 72 C_{NTs}. Note that all the observed C_{NTs} have been taken into account whatever the powder (CA1 or CA4) because significant differences in numbers of walls or diameters were not found. About 20% of the observed C_{NTs} are SWNTs and the great majority of the observed MWNTs has only two or three walls, the two-walled C_{NTs} being widely the most frequent. All the inner diameters are smaller than 7 nm (Fig. 6b), the most frequent being 2 nm and more than 20% in the 0.8–1.5 nm range. As illustrated in Fig. 5c–f, the smaller inner diameters rarely correspond to SWNTs: 0.8 nm for two- or three-walled C_{NTs} vs. 1.2 nm for SWNTs. The outer diameters are only slightly larger (Fig. 6b), with a peak in the distribution at 2–3 nm, in agreement with the few number of walls of most C_{NTs}.

4. Discussion

XRD and Mössbauer results show that the calcination at 1100°C (1 h or 10 min) of the $Al_{2-2x}Fe_{2x}O_3$ amorphous solid solution lead to powders which contain, besides an α-$Al_{2-2x}Fe_{2x}O_3$ ($x < 0.1$) solid solution, traces of a Fe-rich phase α-$Fe_{2-2y}Al_{2y}O_3$. The decrease of the calcination temperature to 1050 or 1025°C seems to avoid this phase partitioning. At the same time, the surface area of the powder is increased, up to 8.1 m^2/g for OA1, probably because a higher porosity of the grains is maintained. Thus, the differences between the characteristics of the four CA powders are consequences of both the occurrence or not of phase partitioning and the specific surface area of the starting powder.

Firstly, when some Fe-rich minor phase is present in the starting powder (OA3 or OA4), in comparison with the other ones (obtained from OA1 or OA2), the carbon content is almost unchanged in the corresponding composite powders (CA3 and CA4), but the quantity and quality parameters are lower (C_n, ΔS, and $\Delta S/C_n$, Table 1). Furthermore, some ribbons are detected by SEM in CA4 (Fig. 4 c and d), but not in CA1; whereas, the TEM and HREM observations do not reveal differences between the C_{NTs} or C_{NTs} bundles observed either in CA4 or in CA1. It is obvious that upon reduction, much larger Fe (or Fe_3C) particles are obtained from the Fe-rich minor phase than from the α-$Al_{2-2x}Fe_{2x}O_3$ ($x \leq 0.1$) solid solution. We infer that these large particles catalyze the formation of nontubular carbon forms, such as the large ribbons. They present lower specific surface area than the C_{NTs} or

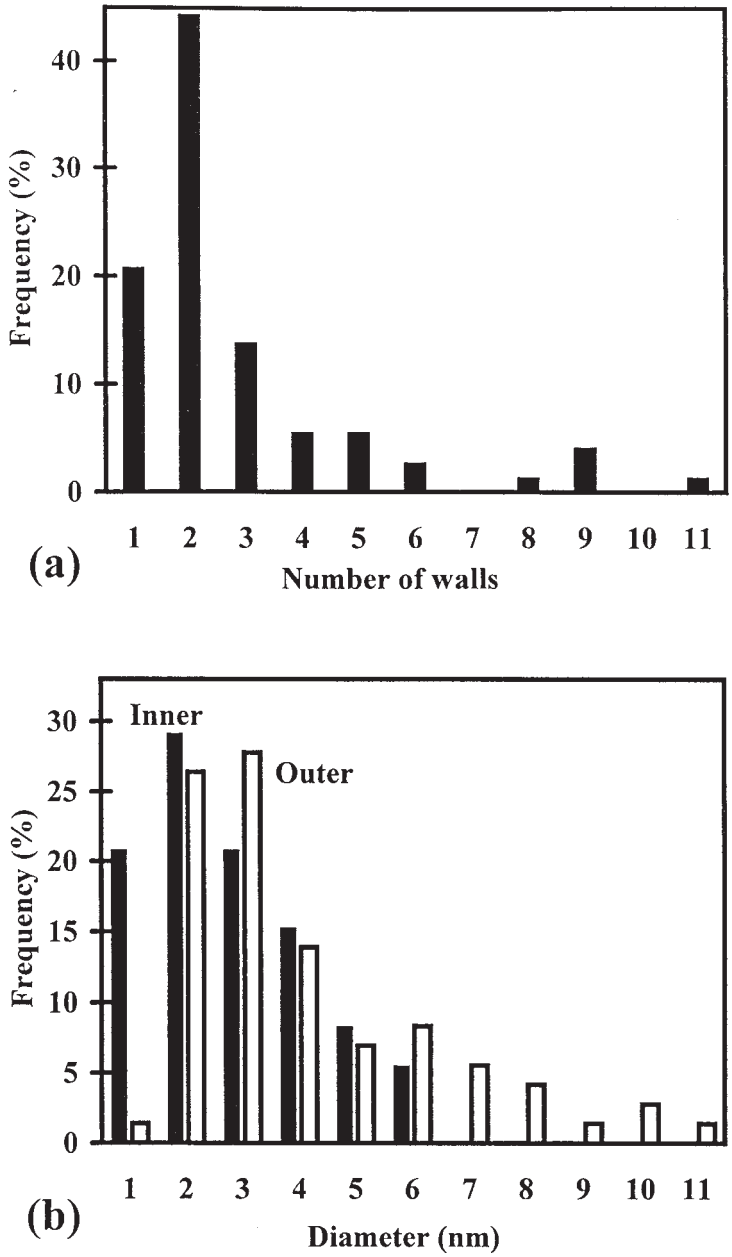

Fig. 6. Distribution of the numbers of walls (a) and of the inner and outer diameters (b) calculated from the observation of 72 carbon nanotubes in HREM digital images.

the C_{NTs} bundles, which explains the smaller ΔS and $\Delta S/C_n$ values (quantity and quality parameters) for the corresponding samples.

Secondly, the specific surface area of the starting powder (S_{ss}) is increased by the decrease of the calcination temperature (and/or time). No Fe-rich phase being detected in the two starting powders (OA2 and OA1), the differences in ΔS and $\Delta S/C_n$ between CA2 and CA1 corresponds to the increase in S_{ss} (Table 1). It was expected that the higher proportion of Fe^{3+} ions located at the surface, which normally gives more surface nanoparticles, would result in more C_{NTs} and thus more carbon. Surprisingly, whereas ΔS increases from CA2 to CA1, the carbon content stays almost constant and thus $\Delta S/C_n$ is increased. The enhancement

of this quality parameter introduces more carbon into either the tubular form or C_{NTs} with fewer walls or smaller diameters. Since, by TEM and HREM, we did not find significant differences in the diameters or number of walls of C_{NTs} between CA4 and CA1, we infer that nontubular carbon species are less easily deposited when more nanoparticles catalyze the formation of C_{NTs}, possibly because less CH_4 is then locally available.

Comparison of CA4 and CB, which differ only by the geometrical surface area of the corresponding starting powder (OA4 and OB), does not reveal significant differences in macroscopic parameters (Table 1, Figs. 2 and 3) or in microscopic characteristics of carbon. Moreover, despite that in OB the gain in geometrical surface area gives a higher proportion of Fe^{3+} ions located at the surface than in OA4, no more carbon content (C_n, Table 1) or carbon surface (ΔS, Table 1) is obtained. Possibly, because the spaces between the grains are much smaller in OB than in the OA powders, the C_{NTs} cannot reach such great lengths in CB as they can in CA powders. It is also possible that there is not enough CH_4 locally and thus some of the Fe nanoparticles cannot catalyze the C_{NTs} formation. However, the web of C_{NTs} bundles surrounds much smaller grains in the CB powder than in the CA powders, which leads to CB presenting an enhanced homogeneity of the repartition between the C_{NTs} and the $Fe/Fe_3C–Al_2O_3$ grains. This will be beneficial for the elaboration of dense C_{NTs}–Fe-Al_2O_3 composites with possibly enhanced mechanical properties.

In our previous works, it was found that a better quality was obtained when the starting powder used contained 5 cat.% Fe rather than 10 cat.% Fe [12]. The optimization of the CH_4 content has led to increase in the macroscopical parameters up to $\Delta S = (6.1 \pm 0.5)$ m^2/g and $\Delta S/Cn = (229 \pm 23)$ m^2/g [16]. In this work, the C_{NTs}–Fe–Al_2O_3 powder labeled CA1 obtained by reduction of a $Al_{1.8}Fe_{0.2}O_3$ starting powder with a high specific surface area (8.1 m^2/g) presents much better parameters: $\Delta S = (19.6 \pm 1.0)$ m^2/g and $\Delta S/C_n = (314 \pm 23)$ m^2/g. Thus, the increase of the Fe content up to 10 cat.% can be beneficial both to the quantity (ΔS) and quality ($\Delta S/C_n$) of the reduced powder. However, this is effective only if the starting powder is, firstly, a pure α-$Al_{2-2x}Fe_{2x}O_3$ solid solution without any trace of a Fe-rich solid solution (α-$Fe_{2-2y}Al_{2y}O_3$) and, secondly, presents the highest specific surface area possible, owing to a low calcination temperature.

The distribution study of the numbers of walls and of diameters of C_{NTs} (Fig. 6a and b) confirms that the catalytic method based on the selective reduction of an oxide solid solution leads to C_{NTs} with small diameters (inner diameter smaller than 7 nm) and fewer walls (1 to 3 for most of them). Indeed, with this method, the Fe nanoparticles nucleate and grow at high temperatures in the CH_4–H_2 gas mixture. At high temperature, they can act as soon as they have the minimal size required for the catalytic formation of C_{NTs}. In contrast, when metal particles are obtained by impregnation of a substrate by the corresponding metal salt solution followed by oxidative and/or reductive heat treatments, they coalesce upon heating up to the temperature of the catalytic decomposition of hydrocarbon or disproportionation of CO. Thus, they catalyze the formation of carbon filaments up to 50 nm in diameter [17,18], some of which are hollow fibers. Moreover, in the ones composed of concentric layers, the number of walls is always very high (often several tens). Fonseca et al. [19], using Co particles prepared by ion adsorption and precipitation on silica, obtained smaller MWNTs, with inner (outer) diameters in the range 4–7 nm (15–25 nm). These results could be explained by an improvement of the repartition of metal particles on the substrate and possibly by a special

interaction particle-substrate. Hafner et al. [20], using Mo or Mo/Fe particles, obtained SWNTs and double-wall CNTs in the diameter range 0.5–3 nm. This was probably due to the nature of the metal or the alloy, either of which is less prone to coalescence than pure Fe, Co, or Ni. Cheng et al. [8] prepared ropes of SWNTs 1.2–2 nm in diameter using Fe particles issued from ferrocene, which were obtained in-situ in a gas flow that reacts with them to form C_{NTs}. Thus, small C_{NTs} with few walls can be obtained by the catalytic method if the catalytic nanoparticles are kept as small as possible at high temperature or, better, if they are obtained in the location and thermodynamic conditions where they are immediately active, as in the method developed by Cheng et al. [8] or in the present method [9,11,12,16]. Moreover, the present method leads to high-quality C_{NTs} in large quantities, since the reduction of 10 g of solid solution gives a C_{NTs}–Fe–Al_2O_3 composite powder containing about 0.5 g of C_{NTs}.

5. Conclusions

We have studied the influence of the calcination temperature and time of a $Al_{1.8}Fe_{0.2}O_3$ amorphous solid solution in order to obtain an α-$Al_{1.8}Fe_{0.2}O_3$ monophased solid solution powder with the highest specific surface area possible. Calcination at 1100°C (1 h or 10 min) leads to powders containing some traces of a Fe-rich phase α-$Fe_{2-2y}Al_{2y}O_3$. Decreasing the calcination temperature to 1050 or 1025°C (10 min) avoids this phase partitioning and increases the surface area of the powder.

Differences relative to the starting powders have a dramatic influence on the macroscopic and microscopic characteristics of the C_{NTs}–Fe–Al_2O_3 composite powders obtained by selective reduction under a H_2/CH_4 gas mixture. Any trace of a Fe-rich solid solution (α-$Fe_{2-2y}Al_{2y}O_3$) leads to large Fe particles (tens of nm) that catalyze the formation of non-nanotubular carbon and thus is detrimental to the quality parameter. The high specific surface area of the α-$Al_{1.8}Fe_{0.2}O_3$ monophased solid solution crystallized at low temperature (1025–1050°C) is beneficial to the quality and quantity parameters of the composite powder.

A statistical study of the numbers of walls and of diameters carried out on 72 C_{NTs} confirms that the present method leads to C_{NTs} with small diameters and few walls: about 20% of the observed C_{NTs} were SWNTs; the majority of the observed MWNTs had only two walls and the inner diameters ranged between 0.8 and 6 nm, with a peak at 2 nm. Indeed, the Fe/Fe_3C nanoparticles nucleate and grow at a temperature where they can act as soon as they have the minimal size required for the catalytic formation of C_{NTs}. Thus, this method allows for production of composite powders containing very large quantities of high-quality C_{NTs}.

Acknowledgments

The authors would like to thank Mr. L. Datas (LCMI) for his assistance in the TEM and HREM observations, which were performed at the Service Commun de Microscopie Electronique à Transmission, Université Paul-Sabatier.

References

[1] S. Iijima, Nature (London) 354 (1991) 56.
[2] M.S. Dresselhaus, G. Dresselhaus, P.C. Eklund, Science of Fullerenes and Carbon Nanotubes, Academic Press, San Diego, 1995.
[3] Ch. Laurent, E. Flahaut, A. Peigney and A. Rousset, New J. Chem. 22 (1998) 1229.
[4] V. Ivanov, A. Fonseca, J.B. Nagy, A. Lucas, P. Lambin, D. Bernaerts, X.B. Zhang, Carbon 33 (1995) 1727.
[5] K. Hernadi, A. Fonseca, J.B. Nagy, D. Bernaerts, A. Fudala, A.A. Lucas, Zeolites 17 (1996) 416.
[6] H. Dai, A.G. Rinzler, P. Nikolaev, A. Thess, D.T. Colbert, R.E. Smalley, Chem Phys Lett 260 (1996) 471.
[7] R. Sen, A. Govindaraj, C.N.R. Rao, Chem Phys Lett 267 (1997) 276.
[8] H.M. Cheng, F. Li, G. Su, H.Y. Pan, L.L. He, X. Sun, M. S. Dresselhaus, Appl Phys Lett 72 (1998) 3282.
[9] A. Peigney, Ch. Laurent, F. Dobigeon, A. Rousset, J Mater Res 12 (1997) 613.
[10] X. Devaux, Ch. Laurent, A. Rousset, NanoStruct Mater 2 (1993) 339.
[11] Ch. Laurent, A. Peigney, A. Rousset, J Mater Chem 8 (1998) 1263.
[12] A. Peigney, Ch. Laurent, F. Dumortier, A. Rousset, J Eur Ceram Soc 18 (1998) 1995.
[13] A. Muan, S. Somiya, J Am Ceram Soc 42 (1959) 603.
[14] A. Rousset, J. Paris, Bull Soc Chim Fr 70 (1972) 3729.
[15] A.D. Polli, F.F. Lange, C.G. Levi, J Am Ceram Soc 79 (1996) 1745.
[16] A. Peigney, Ch. Laurent, A. Rousset, J Mater Chem 9 (1998) 1167.
[17] R.T.K. Baker, N. Rodriguez, Mater Res Soc Symp Proc 349 (1994) 251.
[18] S. Heyrrere, P. Gadelle, Carbon 33 (1995) 234.
[19] A. Fonseca, K. Hernadi, P. Piedigrosso, J.F. Colomer, K. Mukhopadhyay, R. Doome, S. Lazarescu, L.P. Biro, Ph. Lambin, P.A. Thiry, D. Bernaerts, J.B. Nagy, Appl. Phys. A 67 (1998) 11.
[20] J.H. Hafner, M.J. Bronikowski, B.R. Azamian, P. Nikolaev, A.G. Rinzler, D.T. Colbert, K.A. Smith, R.E. Smalley, Chem Phys Lett 296 (1998) 195.